

## Pressurized Interfacial Failure of Soft Adhesives

### Supporting Information

Hares Wahdat,<sup>a</sup> Cathy Zhang,<sup>b</sup> Nicky Chan,<sup>b</sup> and Alfred J. Crosby<sup>a,\*</sup>

*a: Polymer Science and Engineering Department, University of Massachusetts Amherst, Amherst, 01003 MA, USA*

*b: Saint-Gobain Research North America, 9 Goddard Road, Northborough, MA 01532, USA*

*\*Corresponding author: acrosby@umass.edu*

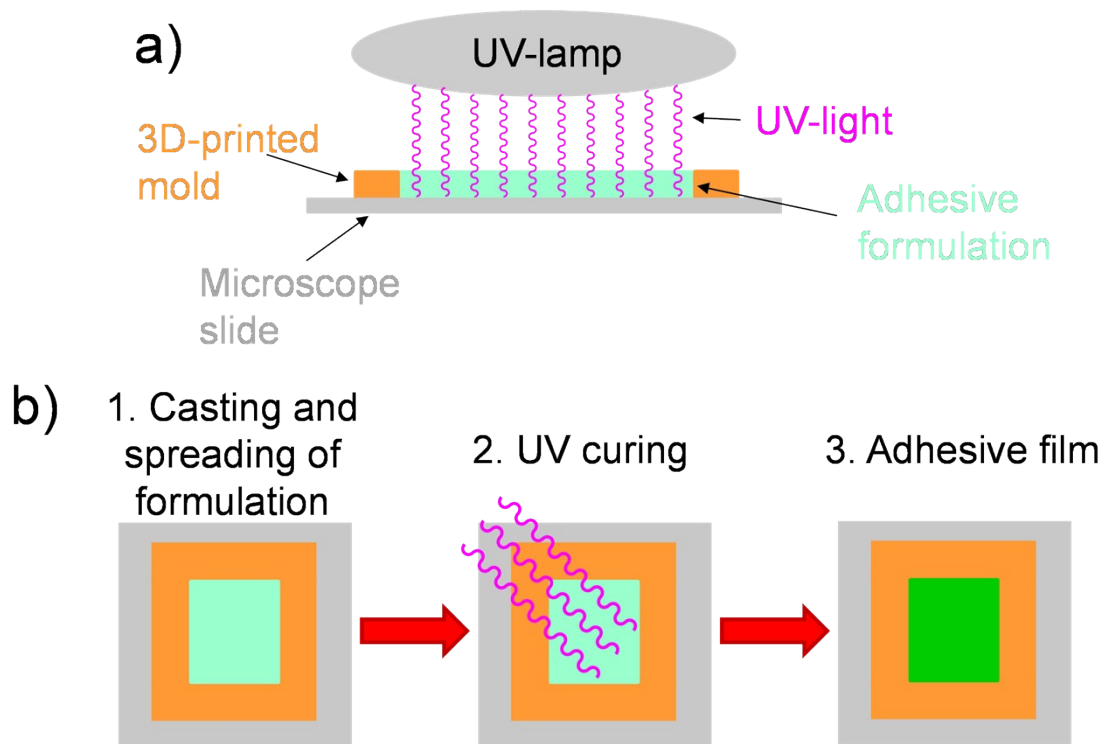
## 1 Preparation and Properties of Materials

### 1.1 Details about Preparation

Acrylic elastomer networks were prepared from UV-curable, liquid formulations. The formulations contained *n*-butyl acrylate (BA), ethylene glycol dimethacrylate (EGDMA), and the photoinitiators Irgacure<sup>®</sup> 184 and Irgacure<sup>®</sup> 819. One formulation was also blended with pre-polymerized, linear poly(*n*-butyl acrylate) (PBA) chains ( $M_w = 96$  kg/mol,  $M_w/M_n = 3.1$ ; determined by gel permeation chromatography (standard: polystyrene, eluent: tetrahydrofuran, temperature: 25 °C)). All chemicals were purchased from Sigma Aldrich, and were used without further purification unless stated otherwise. BA and EGDMA were filtered through alumina filled columns prior to preparing the formulation. PBA chains were dried from a solution in toluene. The solution was first dried overnight at 20 °C, and then in vacuo at 20 °C for three days. The samples are denoted PBAX-*h*. *X* is the weight fraction of the EGDMA cross-linker about the total monomer mass and *h* is the sample's thickness. Unless stated otherwise, both photoinitiators were added at 0.5 wt-% about the total mass of BA and EGDMA each. The composition of the formulations is given in S-Table 1 and its caption.

To prepare the acrylic networks, a volume (200  $\mu$ L for  $h = 300$   $\mu$ m and 500  $\mu$ L for  $h = 1000$   $\mu$ m) of the given formulation was evenly spread over a quadratic area of 400 mm<sup>2</sup> onto a microscope slide (50 mm x 75 mm). The area and thickness of the formulations were controlled by 3D-printed molds that were glued to the microscope slides (see S-Figure 1). The height of the 3D-printed molds was either 0.5 mm (for  $h = 300$   $\mu$ m) or 1 mm (for  $h = 1000$   $\mu$ m). Upon spreading, the formulations were

illuminated by UV-light for photopolymerization. The conditions were: Total energy applied per unit area =  $75 \text{ W}\cdot\text{s}/\text{cm}^2$ , wavelength = 365 nm, intensity = 200 mW, time = 25 min, nitrogen-atmosphere, temperature = 25 °C.



S-Figure 1: Sketch of preparing acrylic adhesives from UV-curable formulations. Wavelength of UV light = 365 nm, intensity = 200 mW and curing time = 25 min. UV-curing occurred under a nitrogen atmosphere.

**S-Table 1: Composition and thickness of acrylic adhesive samples. Both Irgacure® 184 and Irgacure® 819 were added at 0.5 wt-% about the total mass of the monomers each. None of the formulations listed in S-Table 1 contain linear PBA chains. The number in parentheses is the standard deviation.**

Sample	$100 \cdot (m_{\text{EDGMA}}/m_{\text{BA}})$	$h$ [ $\mu\text{m}$ ]
PBA0.25-300	0.25	326 (18)
PBA0.25-1000	0.25	976 (24)
PBA0.5-300	0.5	373 (12)
PBA0.5-1000	0.5	1053 (31)
PBA1-300	1	324 (20)
PBA1-1000	1	1097 (16)

The sample **PBA0.25-300+L** contains linear PBA chains. The composition of PBA0.25-300+L is:  $100 \cdot (m_{\text{EGDMA}}/m_{\text{BA}}) = 0.25$ ,  $m(\text{PBA})/(m(\text{BA})+m(\text{EGDMA})) = 0.22$ . Both Irgacure® 184 and Irgacure® 819 were added at 2.5 wt-% about the total mass of BA and EGDMA each. Thickness of PBA0.25+300-L is 251 ( $\pm$  12)  $\mu\text{m}$ .

## 1.2 Elastic Moduli of Adhesives

The elastic modulus,  $E$ , of each material was determined by probe tack tests at a probe displacement rate of 1  $\mu\text{m/s}$ . Force–displacement curves were measured by the same probe used for the pressurized interfacial fracture experiments, as reported in the main manuscript. The effective modulus,  $E/(1 - \nu^2)$ , was determined from the probe indentation stage in the force–displacement curve following our analysis according to Ref. 1. By assuming a Poisson’s ratio of 0.5 for all materials, the values of  $E$  that are provided in S-Table 2 were calculated.

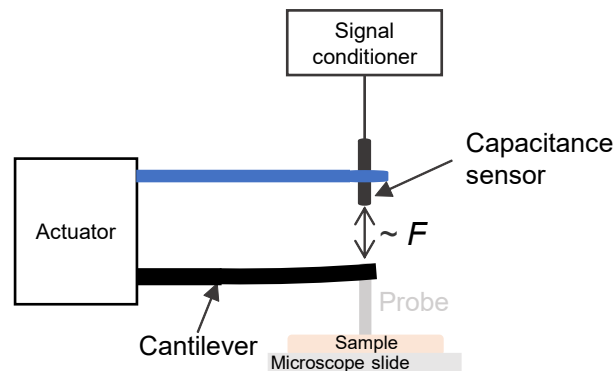
**S-Table 2: Elastic modulus,  $E$ , of all materials. Numbers in parentheses are standard deviations.**

<b>Sample</b>	<b><math>E</math> [kPa]</b>
PBA0.25-300+L	6 (2)
PBA0.25-300	43 (4)
PBA0.25-1000	35 (4)
PBA0.5-300	108 (7)
PBA0.5-1000	94 (1)
PBA1-300	300 (20)
PBA1-1000	268 (9)
VHB1000	81 (3)

## 2 Cantilever-based Load Cell Used in Contact Adhesion Testing

### Instrument

To measure the contact force,  $F$ , in the pressurized interfacial fracture and probe tack tests, the probe was attached to a custom-made cantilever-based load cell as sketched in S-Figure 2. The cantilever was an aluminum sheet. While the probe is in contact with a surface, the cantilever is deflected, and the deflection of the cantilever is proportional to  $F$ . During compression/indentation, the cantilever is bent upwards, and during tension/retraction, it is bent downwards. The deflection of the cantilever is measured by a capacitance sensor (PI D-510 021 Seca, Physik Instrumente, Germany) that is connected to a signal conditioner (PI E-852, Physik Instrumente, Germany).  $F$  was calculated from the cantilever deflection using a linear calibration curve that was determined by placing exact weights



**S-Figure 2: Sketch of the load cell used in the contact adhesion testing instrument for pressurized interfacial fracture and probe tack measurements. Both the aluminum cantilever and the capacitance sensor are attached to an actuator. The capacitance sensor measures a voltage difference between its bottom surface and the top surface of the cantilever. The voltage is proportional to the cantilever deflection from which the force,  $F$ , was calculated. Bending of the cantilever is exaggerated for clarity. The maximum deflection angle as calculated using traditional beam deflection mechanics<sup>2</sup> was never larger than  $0.5^\circ$ .**

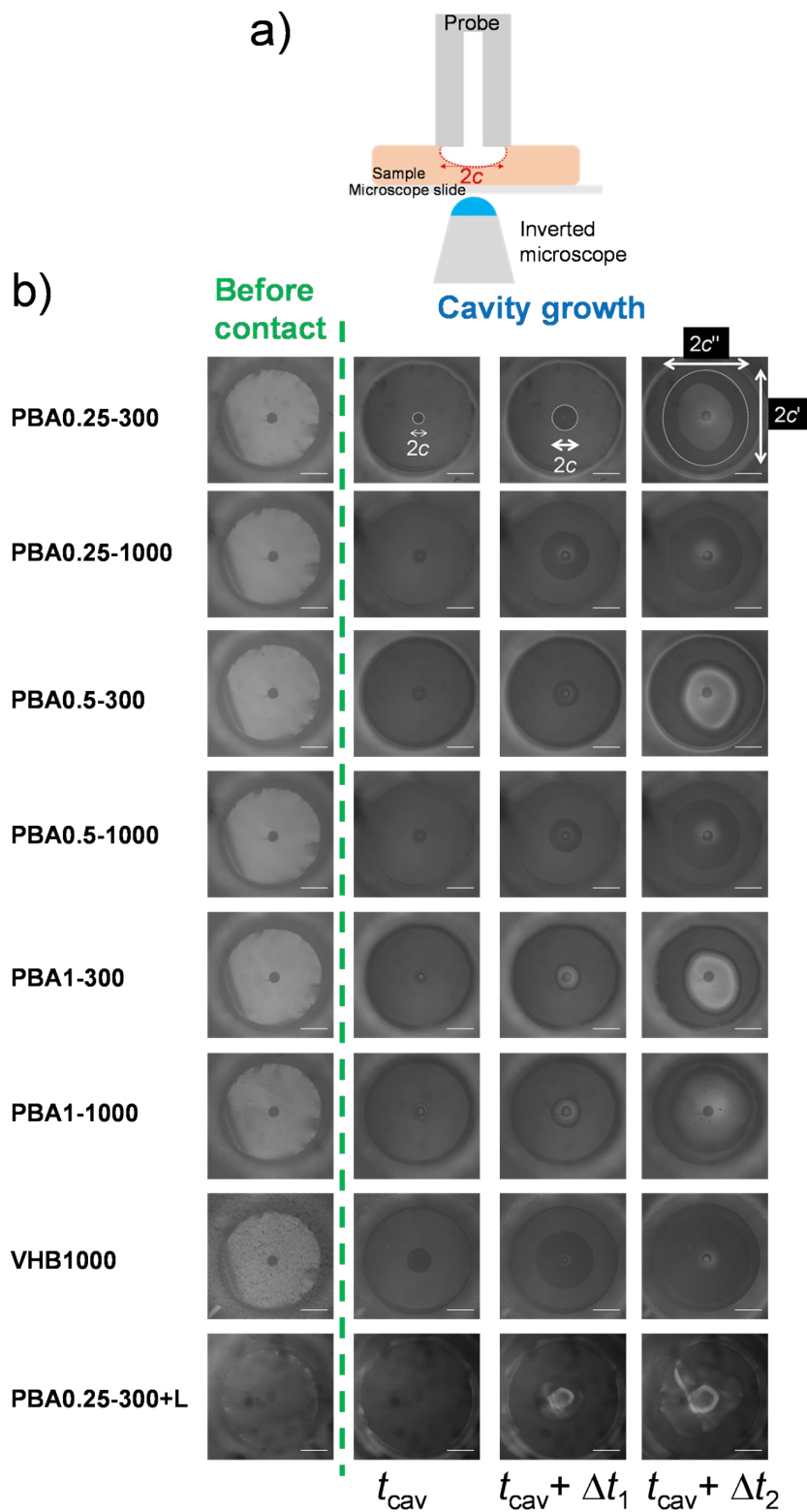
on the cantilever and determining its deflection while it is in contact with air.

The probe displacement is controlled by an actuator (Burleigh Inchworm, Exfo). The true displacement,  $\delta$ , was determined as  $\delta = \delta' - F/K$  with  $\delta'$  being the raw displacement measured by the actuator and  $K$  being the stiffness of the cantilever, which equals the slope of a force–displacement

curve between the probe and a non-adhesive, rigid surface such as a microscope slide. For pressurized interfacial failure (PIF) experiments, two cantilevers were used depending on the maximum contact force. For materials where the maximum contact force during the experiment was 250 mN, a cantilever with a stiffness of around 4 mN/ $\mu\text{m}$  was used, and for higher forces a cantilever with stiffness of around 10 mN/ $\mu\text{m}$  was used. For sphere-probe measurements a cantilever with either 1 mN/ $\mu\text{m}$  or 4 mN/ $\mu\text{m}$  was used, depending on the studied material. All cantilevers provided for a good signal-to-noise ratio. The maximum deflection angle as calculated using traditional beam deflection mechanics<sup>2</sup> was never larger than 0.5°.

### **3 Determination of Cavity Radius from Contact Images**

The cavity radius,  $c$ , was determined from interfacial contact images recorded by an inverted microscope (AxioVert 200M, AxioCam ICc 1) that is placed below the microscope slide to which the sample is attached (S-Figure 3 a). S-Figure 3 b shows contact images for all samples before contact and while the cavity grows. In all cases, the cavity shape was either circular or slightly elliptical. For the analysis conducted in the main manuscript, a circular cavity with radius  $c$  was assumed in all cases. When the cavity had a slightly elliptical shape,  $c$  was taken as the average value of the two radii,  $c'$  and  $c''$ , of the ellipse (S-Figure 3 b).



S-Figure 3: a) Sketch highlighting how contact images were measured in the PIF experiment. b) Evolution of contact images before contact and during cavity growth. All scale bars are 500  $\mu\text{m}$ . Image quality for PBA0.25-300+L is slightly worse because this sample was yellow-colored due to the higher amount of initiator used.  $t_{cav}$  is the time when the cavity starts to form, and  $\Delta t_1$  and  $\Delta t_2$  ( $\Delta t_2 > \Delta t_1$ ) are the times that the cavity has grown. Due to different cavity growth rates, the values of both  $\Delta t_1$  and  $\Delta t_2$  should be compared qualitatively with each other for different samples.

## 4 Determination of Error Bars for Pressure, Force and Cavity Radius

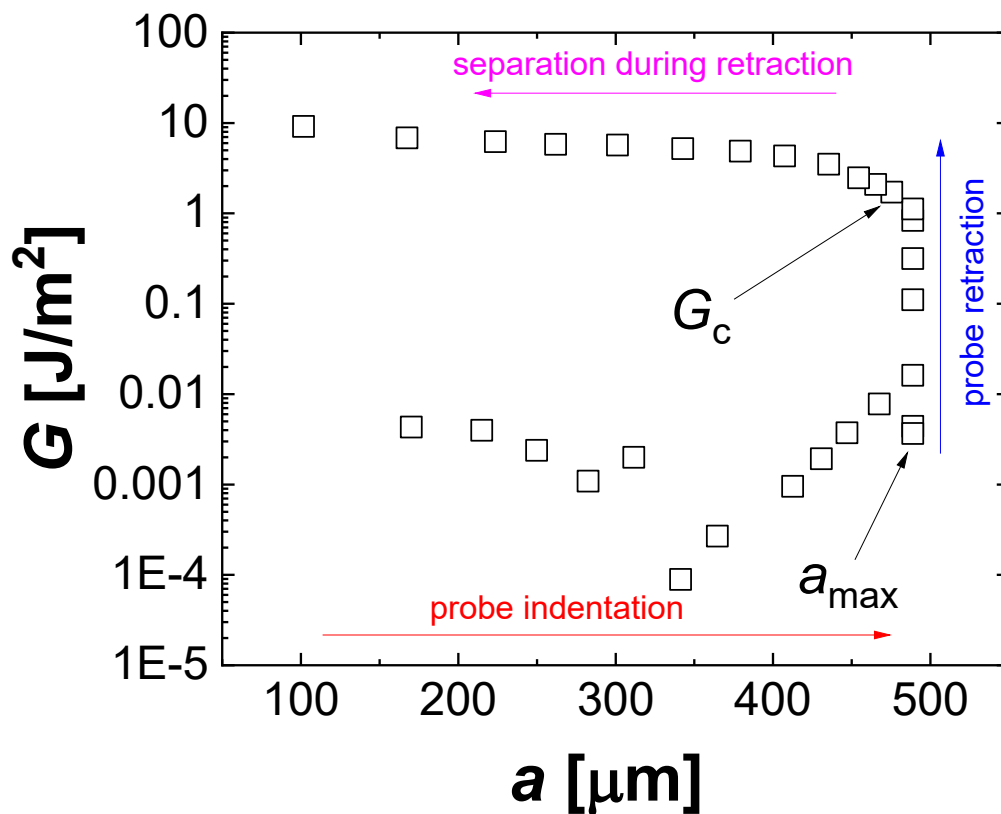
### Interrelationship

The error bars in the plot shown Figure 3 a in the main manuscript for the interrelationship between force, pressure and cavity radius were calculated as follows: For at least three different measurements of the interrelationship between force, pressure and cavity radius for a given material, the relative standard error (RSE) was calculated for pairs of  $x$ - and  $y$ -values covering the entire data set ( $x = (c^2 - b^2)/(a^2 - b^2)$ ,  $y = \Delta F/(p\pi(a^2 - b^2))$  ; notation of variables follows the main manuscript). The RSE was nearly constant over the entire data set. The RSE was averaged, and the standard deviation for the  $x$ - and  $y$ -value of each data point was calculated. The so calculated standard deviation corresponds to the error bars in Figure 3 a in the main manuscript.

## 5 Determination of Critical Energy Release Rate for Detachment by Sphere-probe Tack Tests

To determine the critical energy release rate for detachment,  $G_c$ , sphere-probe tack tests were conducted on all materials. The instrument was the same contact adhesion tester that was used to conduct pressurized interfacial fracture measurements, with the exception that a glass hemisphere with radius of 2.5 mm (Edmund Optics) was used as a probe. Force–displacement curves and contact images were recorded at a probe displacement rate of 1  $\mu\text{m/s}$ .

The critical energy release rate for detachment,  $G_c$ , was determined using the established protocol by Shull *et al.* in Ref. 3. Briefly, from  $F$ ,  $\delta$  and contact radius,  $a$ , the energy release rate  $G$  was calculated. To determine  $G_c$ ,  $G$  was plotted against  $a$  on a semi-log plot as exemplary shown for PBA0.25-300 in S-Figure 4. During the initial stages of probe retraction,  $a$  remains constant at  $a_{\text{max}}$

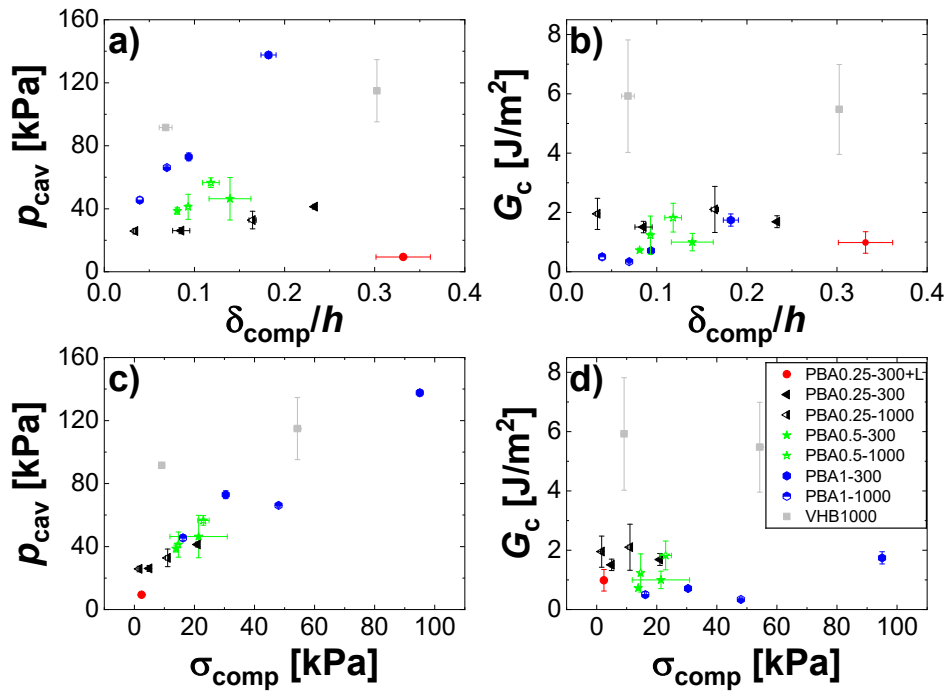


S-Figure 4: Determination of  $G_c$  from sphere-probe tack tests.

while  $G$  increases. At a critical value of  $G$ , interfacial separation starts and  $a$  becomes smaller than  $a_{\max}$ . The first value of  $G$  after  $a < a_{\max}$  was identified with  $G_c$ .

## 6 Influence of Compressive Stress and Displacement on Critical Pressure for Interfacial Cavity Growth

The influence of the compressive strain,  $\delta_{\text{comp}}/h$ , with  $\delta_{\text{comp}}$  the compressive probe displacement prior to cavity formation and  $h$  the sample's thickness, and contact stress,  $\sigma_{\text{comp}} = F_{\text{comp}}/(\pi(a^2 - b^2))$ , with  $F_{\text{comp}}$  being the compressive force at  $\delta_{\text{comp}}$ , on the critical pressure for cavity formation,  $p_{\text{cav}}$  is shown in S-Figure 5 a, c. Increasing both  $\delta_{\text{comp}}/h$  and  $\sigma_{\text{comp}}$  increases  $p_{\text{cav}}$ . However, when comparing the values of  $G_c$  as calculated using the analysis presented in the main manuscript, which accounts for  $\sigma_{\text{comp}}$ , the differences of the  $G_c$  values of each sample when altering  $\delta_{\text{comp}}/h$  by a factor of up to 3 is negligible (S-Figure 5 b, d).



S-Figure 5: Comparison of  $p_{\text{cav}}$  and  $G_c$  for different compressive strains,  $\delta_{\text{comp}}/h$ , and compressive pre-load stresses,  $\sigma_{\text{comp}} = F_{\text{comp}}/(\pi(a^2 - b^2))$ .

## 7 References

1. H. Wahdat, P. Elzière, N. Chan and A. J. Crosby, *Soft Matter*, 2021, **17**, 5540.
2. T. J. Lardner and R. R. Archer, *Mechanics of Solids*, 1st Edition, McGraw-Hill, 1994.
3. A. J. Crosby and K. R. Shull, *J. Polym. Sci. B Polym. Phys.*, 1999, **37**, 3455.